Amendment to the Drawings:

Please replace drawing sheets 3/14, 6/14, 8/14, 9/14 and 10/14 in the Application with the enclosed replacement drawing sheets 3/14, 6/14, 8/14, 9/14, and 10/14.

Remarks

Claims 84-119 are pending in the Application.

Claims 84-117 stand rejected.

Claim 118 is amended herein.

I.   REJECTIONS UNDER 35 U.S.C. § 102(e) OVER *UCHIDA*

Claims 84 and 104 are rejected under 35 U.S.C. § 102(e) as being anticipated by *Uchida et al.*, United States Patent No. 5,560,898 (*"Uchida"*). Office Action, at 2. Applicant respectfully traverses these rejections.

Anticipation requires each and every element of the claim to be found within the cited prior art reference.

Each of Claims 84 and 104 possesses the limitation that the carbon nanotubes are single-wall carbon nanotubes. Single-wall carbon nanotubes are not taught by *Uchida*. The carbon nanotubes of *Uchida* are multi-wall carbon nanotubes. See *Uchida*, cols. 1 & 2. In Example 1, *Uchida* states "Carbon nanotubes were prepared in accordance with the method disclosed in the above-mentioned Ebbesen et al. article." (Ebbesen et al., *Nature*, 358, 220 (1992) is attached as **Exhibit A.**) (*"Ebbesen"*). The carbon nanotubes of *Ebbesen* are multi-wall carbon nanotubes, as stated in *Ebbesen* at 221, col. 1, par. 4 and col. 2, Figure 3.

The distinction between single-wall and multi-wall carbon nanotubes is important because multi-wall carbon nanotubes are fundamentally different from single-wall carbon nanotubes. Single-wall carbon nanotubes have only a single layer of sp^2-hybridized carbon atoms generally arranged in hexagons and pentagons. Because of their single-layer, single-wall carbon nanotubes generally cannot support defects in growth and are more susceptible to destruction by bond breakage or reaction. In contrast, multi-wall carbon nanotubes are composed of multiple, cylindrical concentric carbon layers arranged in a nested or scrolled fashion. Because of this arrangement, the carbon shells of multi-wall carbon nanotubes can withstand wall defects, which often appear as dislocations, kinks, holes, edges on the side-wall

surfaces, *etc.* Also because of their multiple layers and the interconnections between these layers, multi-wall nanotubes can withstand much more rigorous chemical processing, physical conditions, and extensive chemical bond breakage without nanotube destruction compared to single-wall carbon nanotubes. For example, multi-wall carbon nanotubes would be expected to withstand the severe and extensive pulverization process of *Uchida*; however, single-wall carbon nanotubes would be expected to be broken and severely damaged by the procedure.

Further in contrast to multi-wall carbon nanotubes, single-wall carbon nanotubes "rope" together and are held tightly by van der Waals forces. As such, single-wall nanotubes are difficult to separate and disperse in other media, while multi-wall nanotubes generally do not rope and, as such, are readily separable and dispersible. The structural differences between single-wall and multi-wall carbon nanotubes, including the substantial differences in the amount of defects and the roping phenomenon, also lead to significant differences in physical and chemical properties, such as tensile strength, modulus, flexibility, thermal conductivity, electrical conductivity, chemical reactivity and chemical stability. As a result of such differences, the chemistry performed on multi-wall carbon nanotubes can give quite different results from those results obtainable with single-wall carbon nanotubes, such that the physical stability and the chemical reactivity of the former are not accurate predictors of the physical stability and chemical reactivity of the latter. Thus, the physical and chemical properties are quite different and unpredictable, such that one of ordinary skill in the art would not be motivated to apply the processes *Uchida* used with multi-wall carbon nanotubes to that of single-wall carbon nanotubes.

Furthermore, there is no reasonable expectation of success in using the teachings of *Uchida* with single-wall carbon nanotubes. The generally smaller size, and hence higher curvature, bond strain and reactivity, of single-wall carbon nanotubes compared to multi-wall carbon nanotubes, the roping of single-wall carbon nanotubes and the difficulty in dispersing single-wall carbon nanotubes due to their tendency to be held tightly together by van der Waals forces would discourage one of ordinary skill from expecting that the teachings of *Uchida* would give a similar result or be successful with single-wall carbon nanotubes. For example, multi-wall carbon nanotubes would be expected to survive the high temperature calcination conditions of

Uchida; however, air oxidation of single-wall carbon nanotubes at such temperatures would be expected to severely oxidize and destroy the single-wall carbon nanotubes due to their higher reactivity compared to multi-wall carbon nanotubes.

As a result of the foregoing, Applicant respectfully requests that the Examiner withdraw the rejection of Claims 84 and 104 under 35 U.S.C. § 102(e) as being anticipated by *Uchida*.

II.   REJECTION UNDER 35 U.S.C. § 103(a) OVER *UCHIDA* IN VIEW OF *HIURA*

Claims 83-103 and 105-117 are rejected under 35 U.S.C. § 103(a) as being unpatentable over *Uchida* in view of *Hiura et al.*, United States Patent No. 5,698,175 ("*Hiura*"). Office Action, at 3-4. Applicant respectfully traverses this rejection.

Claim 83 had previously been cancelled by preliminary amendment filed on Dec. 21, 2001. Therefore, the rejection of Claim 83 is moot.

To establish a *prima facie* case of obviousness, three basic criteria must be met. First, there must be some suggestion or motivation, either in the references themselves or in the knowledge generally available to one of ordinary skill in the art, to modify the reference or to combine reference teachings. Second, there must be a reasonable expectation of success. Finally, the prior art reference (or references when combined) must teach or suggest all the claim limitations. The teaching or suggestion to make the claimed combination and the reasonable expectation of success must both be found in the prior art and not based on applicant's disclosure. *See* M.P.E.P. 706.02(j); *see also In re Vaeck*, 947 F.2d 488, 20 U.S.P.Q.2d 1438 (Fed. Cir. 1991).

Regarding Claims 84-103 and 105-117, each of these claims either requires single-wall carbon nanotubes or depends directly or indirectly from a claim requiring single-wall carbon nanotubes. Neither *Uchida* nor *Hiura* teaches or suggests the use of single-wall carbon nanotubes in their processes. Thus, the prior art references, either alone or in combination, do not teach or suggest all of the claimed limitations. In fact, *Hiura* also teaches the very same multi-wall carbon nanotubes as *Uchida*, *i.e.* synthesized by the method of *Ebbesen*, cited above. That the nanotubes of *Hiura* are multi-wall carbon nanotubes is also clearly apparent in *Hiura*, Figure 3. Neither *Uchida* nor *Hiura*, either alone or in combination, provides any suggestion or

motivation to modify the reference or combine the reference teachings, and had there been any suggestion or motivation, the combination would not have yielded the claims of the present invention. The arguments presented above with regard to *Uchida* relating the numerous and substantial differences between single-wall carbon nanotubes and multi-wall carbon nanotubes are also applied here.

Furthermore, had there been a suggestion or motivation to combine the references, there would not be any reasonable expectation of success in combining the teachings of *Uchida* with those of *Hiura*. The structural differences, including the amounts and types of structural defects, between single-wall carbon nanotubes and multi-wall carbon nanotubes, cause significant differences in their chemical and physical properties. For example, the air calcination of *Uchida* at 750°C, when applied to single-wall carbon nanotubes would have been expected to severely damage and ultimately destroy the single-wall nanotubes. In contrast, multi-wall carbon nanotubes, because of their multiple layers and multi-wall structure, are able to withstand such calcination conditions. Individuals skilled in the art recognize the differences between single-wall and multi-wall carbon nanotubes and appreciate the inherent pitfalls associated with drawing analogies between the single-wall and multi-wall carbon nanotubes.

Application of the teachings of *Uchida* and *Hiura* to multi-wall carbon nanotubes, typically riddled with defects, results in the breaking of carbon-carbon bonds generally at regions of defects on the walls as well as the tips. See *Hiura* at Figure 3. However, because of their multi-wall structure, the multi-wall nanotubes can withstand attack to their wall layers and still remain intact. As will be appreciated by one of skill in the art, such bond splitting with single-wall carbon nanotubes would be expected to result in destruction of the single-wall nanotubes. Hence, not only would the teachings of *Uchida* and *Hiura* not have suggested a reasonable likelihood of success as applied to single-wall carbon nanotubes, such a chemical protocol would fail to achieve the desired results.

Rather than expect the processes of *Uchida* and *Hiura* to succeed in purifying the single-wall carbon nanotubes, it was reasonable to believe such processes would destroy the single-wall carbon nanotubes. Such an expectation was, in fact, widely held by those skilled in the art well

after the publication dates of *Uchida* and *Hiura*, as is confirmed by Dujardin *et al.*, "Purification of Single-Shell Nanotubes," *Adv. Mater.*, **10**, No. 8, 611-613 (1998) ("*Dujardin*"), attached as **Exhibit B**. *Dujardin* notes that "[i]t was believed that purification of single-shell nanotubes based on preferential oxidation and/or separation using surfactants was much more difficult that that of [multi-shell] nanotubes." *Dujardin*, at 611. A reason for this was because "gas-phase oxidation, which yields purified multishell nanotubes, destroys the single-shell nanotubes before anything else in the sample." *Id.* Accordingly, a person of ordinary skill would not have been motivated, nor had reason to expect success, in combining the methods of *Uchida* and *Hiura*. And, had a person of ordinary skill combined the references, the combination would not have resulted in the invention of the instant application recited in Claims 84-103 and 105-117.

Thus, as there is no suggestion or motivation in *Uchida*, *Hiura*, or in the knowledge generally available to one of ordinary skill in the art, to modify the references or to combine reference teachings, and, furthermore, as there is no reasonable expectation of success were the references so modified, a *prima facie* case of obviousness is unsupported.

In light of the foregoing, Applicant respectfully requests that the Examiner withdraw the rejection of Claims 84-103 and 105-117 under 35 U.S.C. §103(a) as being unpatentable over *Uchida* in view of *Hiura*.

IV.   CLAIMS 118 AND 119

Claims 118 and 119 are pending in the Application, however, these claims have not been cited or addressed by the Examiner. Claim 118 was amended herein to correct a typographical error. The amendment removes the duplicated word "the" in Claim 118.

V.   AMENDMENTS TO THE DRAWINGS

The present application and United States Patent Application Serial No. 10/027,568, filed December 21, 2001 ("the '568 Patent Application") are both divisional patent applications of the United States Patent Application Serial No. 10/000,746, filed November 30, 2001, all of which applications are commonly assigned. On October 7, 2002, a Notice of Allowance was

transmitted to Applicant for the '568 Patent Application; and Applicant paid the issue fee on October 16, 2002. Subsequently, on March 20, 2003, Applicant received a Notice Regarding Drawings for the '568 Patent Application. Specifically, the Draftperson's review objected to the drawings for Figures 2A-C, 4A-D, 6, and 7A-B for the following reasons set forth on PTO Form 948, which was attached to the Notice Regarding Drawings for the '568 Patent Application. These were:

(a)   Under 37 C.F.R. § 1.84(i), for Figures 2A-C, 4A-D, 6, and 7A-B, "[l]ines, numbers & letters not uniformly thick and well defined, clean, durable, and black (poor line quality)."

(b)   Under 37 C.F.R. § 1.84(m), for Figures 2A-C, 4A-D, 6, and 7A-B, "[s]olid black shading not permitted."

(c)   37 C.F.R. § 1.84(p), for Figures 4A-D, 6, and 7A-B, "[n]umbers and reference characters not plain and legible."

On May 19, 2003, Applicant filed its Response to Notice Regarding Drawings in the '568 Patent Application. In this response, Applicant replaced new drawing sheets 3/14, 6/14, 8/14, 9/14 and 10/14 for the original sheets. These sheets include more legible Figures 2A- 2C, 4A- 4D and 6 – 7B as requested by the Draftsperson. in the Notice Regarding Drawings for the '568 Patent Application.

As the present Application contains these same drawings, Applicant is submitting these improved figures in the present Application. Pursuant to 37 C.F.R. 1.84(b), the improved figures are submitted as photographs, as this is the only practicable medium for illustrating these figures.

Applicant has amended the drawings to facilitate prosecution of the present Application; Applicant believes by doing so, this will obviate this potential issue with the figures.

VI.   AMENDMENTS TO THE SPECIFICATION

After Applicant filed its Response to Notice Regarding Drawings in the '568 Patent Application, Applicant received a Notice of Drawing Inconsistency with Specification in the '568 Patent Application, dated June 2, 2003. In this Notice, Applicant was informed that the

USPTO had received the improved figures (which presumably were accepted by the draftsperson) but the USPTO had now identified an inconsistency between the drawings and the Brief Description of Drawings in the '568 Patent Application. These were: The Brief Description referred to Figures 3A-3B and 5A-5B while the drawings contained Figures 3A-3C and 5A-5C. On June 30, 2003, Applicant filed its Amendment in Response to Notice of Drawing Inconsistency with Specification in the '568 Patent Application. In that amendment, Applicant amended the Brief Description of Drawings and the Detailed Description of the Invention, in the identical manner as presented on page 2 above.

Because this same issue exists in the present Application, Applicant is amending the specification in the same manner as it did in the '568 Patent Application. Accordingly, in the specification, the paragraphs within the Brief Description of Drawings have been amended to correctly identify the drawings. In the Detailed Description of the Invention of the Specification, the amendment of the paragraph beginning at page 18, *l.* 11, was made to harmonize the written description and the drawings. No new matter is added by these amendments to the specification.

The Applicant believea this amendment reconciles the inconsistency between the drawing and the Brief Description of the Drawing. Again, Applicant is amending the specification to facilitate prosecution of the present Application. Applicant believes by doing so, this will obviate this potential issue between the drawings and the specification.

VII.   CONCLUSION

As a result of the foregoing, it is asserted by Applicant that the claims in the Application are now in condition for allowance, and respectfully requests allowance of such claims.

Applicant respectfully requests that the Examiner call Applicant's attorney at the below listed number if the Examiner believes that such a discussion would be helpful in resolving any remaining problems.
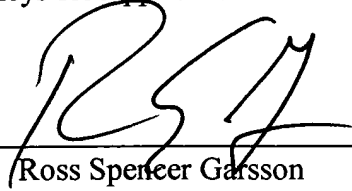
11321-P011C1D1

PATENT

Respectfully submitted,

WINSTEAD SECHREST & MINICK P.C.

Attorneys for Applicant

By:_____
/Ross Spencer Garsson
Reg. No. 38,150

P.O. Box 50784
Dallas, Texas 75201
(512) 370-2870

similar results but seemed to yield less accurate predictions than the interpolative approach.

For periodic signals with additive uncorrelated noise, the correlation coefficient is independent of the prediction time. A fall in the correlation with prediction time does not indicate a periodic signal with additive noise, but it may indicate a chaotic signal with or without noise (in the chaotic case, additive noise produces a constant offset in the correlation which would not obliterate the fall-off). Our work provides the means to go one step further and decide whether such a fall-off is indicative of a random fractal sequence. A direct approach will be to check the scaling behaviour of $\log(1 - r(t))$ against t and of $\log(1 - r(t))$ against $\log t$. For example, Fig. 3 shows results from a time series of the Southern Oscillation Index, which is derived from the mean sea-level pressure difference between the Tahiti and Darwin stations. The record is 1,248 values long (monthly values from January 1883 to December 1986) and is related to the El Niño which is hypothesized to be chaotic[16]. A dimension of around five has been suggested for this type of data[17]. Figure 3a is a semi-log plot and Fig. 3b a log–log plot of $1 - r(t)$ against t. The solid lines indicate best fits. For the semi-log plot the best fit is linear, whereas for the log–log plot it appears to be non-linear. According to our theory this indicates that the time series is indeed chaotic. In some cases, noise, data imperfections and data length may make the identification of the actual scaling

difficult. In such cases nonlinear prediction could be used statistically. For example, if a time series is suspected to be a FBM, then prediction results could be compared with the average prediction properties of the family of FBMs in question. □

1. Sugihara, G. & May, R. M. Nature 344, 734–741 (1990).
2. Wales, D. J. Nature 350, 485–488 (1991).
3. Tsonis, A. A. & Elsner, J. B. Nature 333, 545–547 (1988).
4. Essex, C., Lookman, T. & Nerenberg, M. A. H. Nature 326, 64–66 (1987).
5. Frank, G. W., Lookman, T., Essex, C. & Nerenberg, M. A. H. Physica D46, 427–438 (1990).
6. Schaffer, W. M., Olsen, L. F., Truty, G. L., Fulmer, S. L. & Graser, D. J. in From Chemical to Biological Organization (eds Marcus, M., Muller, S. C. & Nicolis, G.) (Springer, New York, 1988).
7. Grassberger, P. & Procaccia, I. Physica D9, 186–208 (1983).
8. Grassberger, P. & Procaccia, I. Phys. Rev. Lett. 50, 346–349 (1983).
9. Osborne, A. R. & Provenzale, A. Physica D35, 357–381 (1989).
10. Theiler, J. Phys. Lett. A155, 480–492 (1991).
11. Farmer, J. & Sidorowich, J. J. Phys. Rev. Lett. 62, 845–848 (1987).
12. Casdagli, M. Physica D35, 335–356 (1989).
13. Rumelhart, D. E., Hinton, G. E. & Williams, R. J. Nature 323, 533–536 (1986).
14. Wolpert, D. M. & Miall, R. C. Proc. R. Soc. B242, 82–86 (1990).
15. Anderson, T. W. An Introduction to Multivariate Statistics (Wiley, New York, 1958).
16. Valis, G. K. Science 232, 243–245 (1986).
17. Hense, A. Beitr. Phys. Atm. 60, 34–47 (1987).

Large-scale synthesis of carbon nanotubes

T. W. Ebbesen & P. M. Ajayan

Fundamental Research Laboratories, NEC Corporation, 34 Miyukigaoka, Tsukuba 305, Japan

INTEREST in carbon fibres[1,2] has been stimulated greatly by the recent discovery of hollow graphitic tubules of nanometre dimensions[3]. There has been much speculation about the properties and potential application of these nanotubes[4–8]. Theoretical studies predict that their electronic properties will depend on their diameter and degree of helicity[4,5]. Experimental tests of these ideas has been hampered, however, by the lack of macroscopic quantities of the material. Here we report the synthesis of graphitic nanotubes in gram quantities. We use a variant of the standard arc-discharge technique for fullerene synthesis under a helium atmosphere. Under certain conditions, a carbonaceous deposit forms on one of the graphite rods, consisting of a macroscopic (diameter of about 5 mm) cylinder in which the core comprises pure nanotubes and nanoscale particles in high yield. The purity and yield depend sensitively on the gas pressure in the reaction vessel. Preliminary measurements of the conductivity of the bulk nanotube material indicate a conductivity of about $100 \, \text{S cm}^{-1}$.

The carbon arc experiments are done in a reaction vessel through which an inert gas (He, Ar and so on) flows at a controlled pressure. We apply a potential of ~18 V, either a.c. or d.c., between two graphite rods (one 6 mm and the other 9 mm in diameter) in the vessel. As the rods are brought close together a discharge occurs resulting in the formation of a plasma. As the smaller rod is consumed, the rods are kept at a constant distance from each other of ~1 mm. On the larger rod, a carbonaceous deposit forms which may contain nanotubes under the right conditions. The electric current depends on the size of the rods, their separation, the gas pressure and so on, but typically it is ~100 A. It was while trying to prepare derivatives of fullerenes under helium atmosphere and alternating current that we discovered how to make nanotubes in reasonable quantities. The techniques were then optimized as described below.
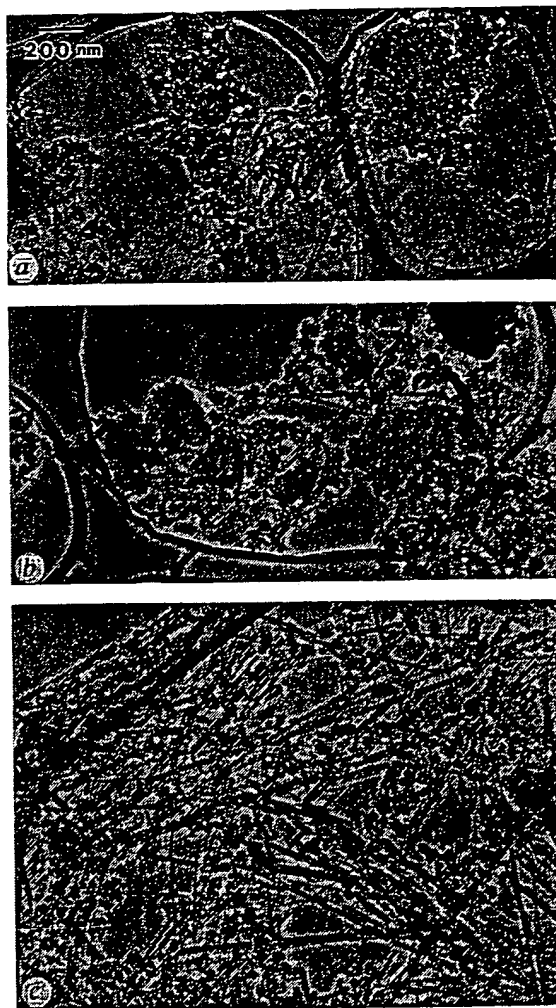

FIG. 1 Low-magnification electron micrographs of samples prepared in helium atmosphere at pressures (a) 20 torr, (b) 100 torr and (c) 500 torr. There is a striking increase in the number of tubes as the pressure increased.

To optimize the yield of nanotubes, we varied conditions such as the type of inert gas, the nature of the current (a.c. or d.c.), the voltage and the relative rod size. The relative yield of nanotubes was monitored by transmission electron microscopy after grinding the carbonaceous deposit and sonicating it in methanol. Figure 1 shows the effect of helium pressure on the yield of nanotubes at 18 V d.c. At 20 torr, hardly any nanotubes can be found. Only amorphous, sheet-like and glassy graphitic material is formed. At 100 torr (Fig. 1b), a few nanotubes appear in the sample. At 500 torr (Fig. 1c) the entire sample consists of carbon nanotubes and nanoparticles (cage structures). We tested the effect of increasing the pressure to 2,500 torr, but the quality of the sample did not change significantly. The amount of recovered material, however, did decrease. Therefore at 500 torr the total yield of nanotubes as a proportion of graphitic starting material is optimal. Under those conditions, ~75% of the consumed graphite rod is converted to a deposit of cylindrical shape and similar diameter.

Figure 2 shows the typical rod-shaped deposit together with the large 9-mm graphite rod on which it forms. The rate at which the rod deposit forms depends on the gas pressure; in the best conditions for producing nanotubes, it is a few millimetres per minute. Two distinct regions can be seen in the cross-section (Fig. 2, inset): an inner black core made only of nanotubes and nanoparticles, and an outer grey metallic hard shell in which no nanotubes are seen by transmission electron microscopy. In other words, the deposit forms a macroscopic tubular structure packed with nanotubes. This preparation method is therefore convenient, as the core can easily be separated from the shell. The weight ratio of the core to the shell is ~1 to 2, corresponding to a nanotube-to-particle yield of 25% of the starting material. This compares favourably to the yield for fullerenes, typically a few per cent of the starting material and 8% of the recovered soot. Within the sample the ratio of tubes to particles is at least 2 to 1 by weight; treating the sample in an ultrasonic bath can free many tubes from the particles which are originally stuck together. The deposit containing the nanotubes is pitch black, but grinding and smearing it over a surface produces a shiny greyish metallic lustre.

We can also prepare nanotubes using alternating current, or in argon (d.c. or a.c.), but the total yields are much smaller. The reason for this might be that the nanotubes are only formed during one part of the a.c. cycle, so the yield is reduced. The inert gas pressure remains critical in all cases and should be 500 torr or larger. We varied the applied potential between 10 V and 18 V, but found that it has little effect on the quality of the sample provided that a plasma is formed.

The carbon nanotubes have the structures reported by Iijima[3] and typically consist of two or more concentric shells of carbon sheets (Fig. 3). The diameter of the nanotubes in our samples ranges between 2 and 20 nm, whereas the lengths are several micrometres. The tips of the tubes are capped with pentagons, giving unique angular relationships between the tube surfaces
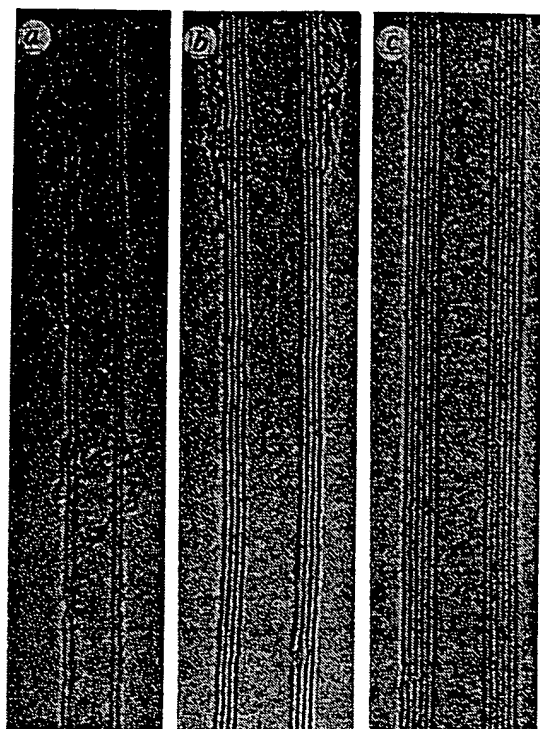

FIG. 3 High-resolution electron micrographs of typical tubes present in samples prepared under helium at 500 torr as described in the text. The number of layers ranges from two to many. The distance between consecutive carbon layers in the tubes is 0.34 nm.

and the tips[9], and a stacked morphology is often seen for the inner structure.

The core material containing the nanotubes is macroscopically fibrous, with the fibres parallel to the direction of the current, suggesting that the nanotubes themselves might be aligned in the sample. Preliminary scanning electron microscope studies support this observation. The fact that nanotubes are found only in the core of the sample and not on the colder edge indicates that the temperature and cooling rate are critical for their formation. This is supported by the importance of the inert gas pressure in the chamber. We also observed that if the plasma is stable, a more even sample is produced. This is similar to the situation of vapour-grown crystals and suggests that with accurate control of the plasma temperature and its uniformity, the diameter and length of the nanotubes could be more precisely controlled. Another possible way of narrowing the distribution of nanotubes is by separating them after formation. This seems to be more difficult than purifying C_{60} from larger fullerenes, when standard chromatography methods can be used. Separation of the nanotubes from the nanoparticles is easier because of the difference in size and shape.

Theoretical calculations predict that a tubular structure is energetically more favourable than a flat sheet of carbon hexagons of width equal to the circumference[6]. The fact that we observe no small sheets or sheet aggregates in our pure samples supports this. Other calculations on the electronic structure of nanotubes predict semiconductor or metallic properties depending on their diameter and helicity[4,5]. Although we have not yet been able to measure the properties of single tubes, the bulk material is indeed conducting with a conductivity larger than $100 \, S \, cm^{-1}$. Considering the discontinuity and diversity in the bulk structure, some tubes must have a much higher conductivity than this average value.

The ability to mass-produce nanometre fibrous materials with large aspect ratios (length/diameter), such as the carbon nanotubes, is of importance in materials science[10]. Our
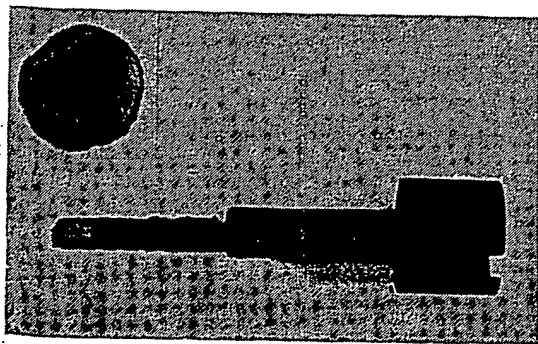

FIG. 2 Rod-shaped deposit, together with the larger graphite rod on which it forms. Inset: cross-section of the deposit (diameter ~5 mm).

large-scale synthesis method for nanotubes is simple and easily accessible to others with an interest in this novel material, and should enable studies to be undertaken to evaluate their physical properties and assess potential applications in areas such as catalysis, composite materials and nanowires.   □

1. Speck, J.S., Endo, M. & Dresselhaus, M. S. *J. Cryst. Growth* **94**, 834–848 (1989).
2. Tibbits, G. G. *J. Cryst. Growth* **66**, 632–638 (1984).
3. Iijima, S. *Nature* **354**, 56–58 (1991).
4. Mintmire, J. W., Dunlap, B. I. & White, C. T. *Phys. Rev. Lett.* **68**, 631 (1992).
5. Hamada, N., Sawada, S. & Oshiyama, A. *Phys. Rev. Lett.* **68**, 1579–1581 (1992).
6. Sawada. S. & Hamada, N. *Solid State Commun.* (in the press).
7. Robertson, D. H., Brenner, D. W. & Mintmire, J. W. *Phys. Rev.* (in the press).
8. Adams, G. B. *et al. Science* (in the press).
9. Iijima, S., Ichihashi, T. & Ando, Y. *Nature* **356**, 776–778 (1992).
10. Calvert, P. *Nature* **357**, 365–366 (1992).

Negative Poisson ratios in crystalline SiO₂ from first-principles calculations

Nitin R. Keskar & James R. Chelikowsky

Department of Chemical Engineering and Materials Science,
Minnesota Supercomputer Institute, University of Minnesota,
Minneapolis, Minnesota 55455, USA

THE Poisson ratio of a solid characterizes its response to uniaxial stress. It is defined as the negative ratio of the transverse strain to the corresponding axial strain. Normally, this ratio is positive, as most solids expand in the transverse direction when subjected to a uniaxial compression. Although a negative Poisson ratio is not forbidden by thermodynamics, it is rare in crystalline solids: the results of recent experiments[1] which observed a negative Poisson ratio in α-cristobalite were therefore unexpected. We have investigated the elastic behaviour of α-cristobalite and other forms of silica with first-principles calculations and classical interatomic potentials. Our calculations reproduce the negative Poisson ratio in α-cristobalite, and predict that α-quartz, the most common form of crystalline silica, will also exhibit a negative Poisson ratio under large uniaxial tension. We attribute the occurrence of a negative Poisson ratio in low-density silica polymorphs to the high rigidity of the SiO₄ tetrahedra.

For a crystal with a tetragonal or hexagonal unit cell defined by the lattice parameters a and c, the Poisson ratio for a uniaxial loading along the c-axis is given by

$$\sigma = -\frac{\Delta a/a}{\Delta c/c} = -\frac{\Delta \ln(a)}{\Delta \ln(c)} \quad (1)$$

Solids under such conditions usually deform to conserve volume: compression in one direction results in an expansion in the transverse direction. This gives a positive Poisson ratio. An empirical rule of $\sigma > 0$ is satisfied by virtually all known solids. A negative value of Poisson ratio is not forbidden: the requirement that the strain energy for an elastic isotropic solid be non-negative leads only to the restriction $-1 \leq \sigma \leq \frac{1}{2}$. For an anisotropic solid, the allowed range is even wider[2]. Two examples of metallic crystal systems with negative Poisson ratios are known[3,4]. It is difficult to measure a negative Poisson ratio, and the observation of such a ratio can be spurious[5]. A theoretical confirmation can validate experimental results, but such calculations have been rare.

Weidner *et al.*[1] have recently measured single-crystal elastic moduli of α-cristobalite. The polycrystalline aggregate values of the moduli were: bulk modulus $B = 16.4$ GPa; shear modulus $G = 39.06$ GPa. These values result in a Poisson ratio of -0.16
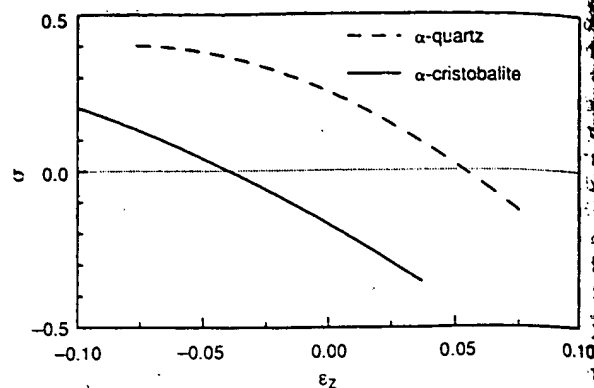

FIG. 1 Variation of the Poisson ratios of α-quartz and α-cristobalite as function of uniaxial strain along the c-axis. This figure is based on pair-potential calculations. Note that a positive strain occurs for a material under tension.

for α-cristobalite according to the following relationship isotropic materials:

$$\sigma = \frac{3B - 2G}{2(3B + G)}$$

This result was certainly counterintuitive. α-cristobalite is covalent polymorph of silica in which the silicon cations fourfold coordinated. It has the same basic building block SiO₄ tetrahedra, as other common forms of crystalline silica such as α- and β-quartz. The latter crystals are reported to have a positive Poisson ratio at ambient pressure[6].

We analysed the Poisson ratio of crystalline silica using two theoretical approaches. One approach is based on classical interatomic potentials. The other is based on *ab initio* pseudopotentials and is fully quantum-mechanical. The classical pair potential that we have used in this study was developed using Hartree–Fock self-consistent calculations on SiO₄ clusters[7]. This interatomic potential seems to work well for structural and elastic properties of silica structures[7,8], but one might not expect it to work for details of the elastic properties of silica, especially for open structures where angular forces might be important. To verify the results we used quantum-mechanical calculations. These calculations give accurate structural properties, but they are computationally intensive. We have used 'soft' pseudopotentials constructed within the local density approximation[9]. These pseudopotentials are widely applicable and transferable[9,10]. Details of the methods can be found elsewhere[11-13].

Determining the Poisson ratio of α-cristobalite is complicated by its large unit cell and the number of degrees of freedom the atoms. α-cristobalite has a tetragonal unit cell which completely defined by lattice parameters a and c, and the internal coordinates u, x, y and z (ref. 14).

In calculating the Poisson ratio, we used the definition equation (1). For a fixed value of c, we let the other lattice parameter and internal coordinates relax to find a minimum energy structure. We then changed the values of c and let the internal coordinates and a relax to find the minimum-energy structure for the new value of c. Owing to the computational difficulties of this energy minimization, we optimized geometries using pseudopotential calculations at only four values of c. our pair-potential calculations, we examined the structure at values of the lattice parameter c. This procedure gives us the energy of the structure and the lattice constant a as a function of the lattice constant c for a material under a uniaxial stress.

In Fig. 1, we show the variation of the Poisson ratio as function of the engineering strain along the c-axis, defined $\varepsilon_z = (c - c_0)/c_0$. For $\varepsilon_z \geq -0.04$ the Poisson ratio assumes

ADVANCED MATERIALS

Purification of Single-Shell Nanotubes**

By *Erik Dujardin, Thomas W. Ebbesen,* *Ajit Krishnan,* and *Michael M. J. Treacy*

The recent discoveries of methods[1,2] for large-scale synthesis of single-shell nanotubes has opened the door to studying their physical and chemical properties, which are expected to be quite unique.[3,4] However, the samples still contain large amounts of impurities (typically 30 % or more), such as amorphous carbon and catalytic metal particles, that need to be eliminated for accurate measurements, whether one studies the bulk or the individual tubes. Here we report an extremely simple and efficient method for removing most of the impurities from the nanotube samples.

It was believed that purification of single-shell nanotubes based on preferential oxidation and/or separation using surfactants was much more difficult than that of multishell nanotubes.[5–8] For instance, gas-phase oxidation, which yields purified multishell nanotubes,[5] destroys the single-shell nanotubes before anything else in the sample. So efforts have been directed at modifying other techniques originally developed for multishell nanotubes.[9,10] Tohji et al.[9] published a method using ultrasonication in water and treatment with hydrochloric acid. The yield of pure single-shell nanotubes is only 2 % of the starting material for a 48 h process. More recently, Bandow et al.[10] reported a method mainly based on microfiltration under overpressure. A major advantage of this process is that it is driven by pure physicochemical interactions of the carbon products with the amphiphilic molecules and the filter membrane, leaving the nanotubes undamaged. The most serious drawback is the dependence of this procedure on the quality of the sample. It is known that sonicating nanotubes for a long period of time and at a high frequency can cause damage by breaking the nanotubes up into smaller pieces.[11] We have found it hard to successfully apply this method to all samples. Typically, significant amounts of amorphous carbon and catalytic particles remain.

The one-step method presented here does not appear to be sensitive to the quality of the starting material. Moreover, it eliminates at the same time the carbonaceous material and most of the catalytic metal content.

[*]   Prof. T. W. Ebbesen[+]
       ISIS, Louis Pasteur University
       4 rue Blaise Pascal, F-67000 Strasbourg (France)
       E. Dujardin
       Laboratoire de Chimie des Interactions Moléculaires
       Collège de France
       11 place Marcelin Berthelot
       F-75231 Paris Cedex 05 (France)
       Dr. A. Krishnan, Dr. M. M. J. Treacy
       NEC Research Institute
       4 Independence Way, Princeton, NJ 08536 (USA)

[+]   Present address: NEC Research Institute, 4 Independence Way, Princeton, NJ 08536, USA.

The single-shell nanotubes were prepared by the laser-oven ablation method[1] (see Experimental section). In this way, up to 30 mg/h of raw material could be synthesized, providing that the focused laser spot was continuously moved on the target surface to uniformly ablate the superficial material. Among all the parameters of this method, this one seems to be the most critical in order to obtain good yields. The transmission electron microscopy (TEM) pictures in Figure 1 show the quality of such raw single-shell nanotube samples. Typically, there is a mixture of ca. 50 % of bundles of single-shell nanotubes and ca. 50 % of carbonaceous material, gray graphitic nanoparticles, and black catalyst (cobalt and nickel) grains (Fig. 1a). A closer examination (Fig. 1b) of the tubes shows a layer of irregular thickness of amorphous carbon coating the bundles, which is particularly abundant where the bundles cross.

In the desire to open single-shell nanotubes with acids, we processed the raw nanotube samples in boiling concentrated nitric acid (See Experimental section). This method was developed for opening and filling multishell nanotubes by Green and co-workers.[7] To our surprise, the nanotube sample seemed to become purer. After refluxing the sample for
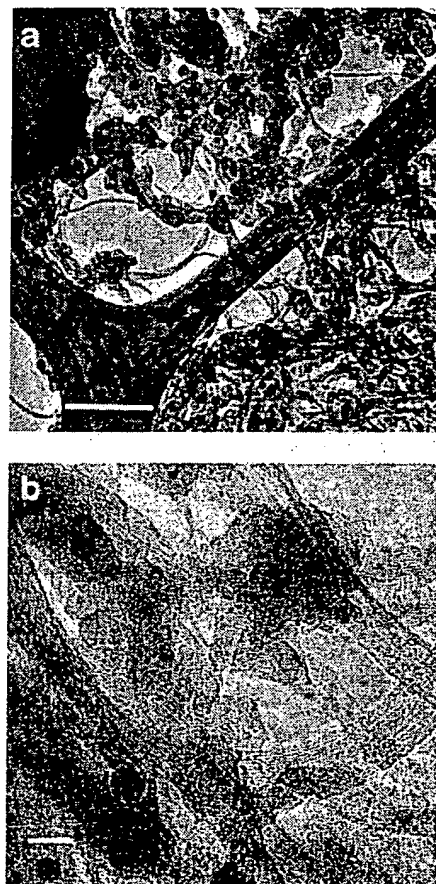

Fig. 1. TEM micrographs at low (a, scale bar 0.2 mm) and high (b, scale bar 20 nm) magnification of as-synthesized single-shell nanotubes. Microscope Hitachi H9000-NAR, 100 kV.

4 h in 70 % nitric acid at 120 °C, it was pure. The result of such a treatment is shown in Figures 2a and 2b. It is striking that the single-shell nanotubes appeared to be sufficiently (chemically) inert for a large proportion to survive such strongly oxidizing conditions. The yields, in terms of left-over weight of the sample after oxidation, can be as high as 50 %, which appears to reflect the initial nanotube content.
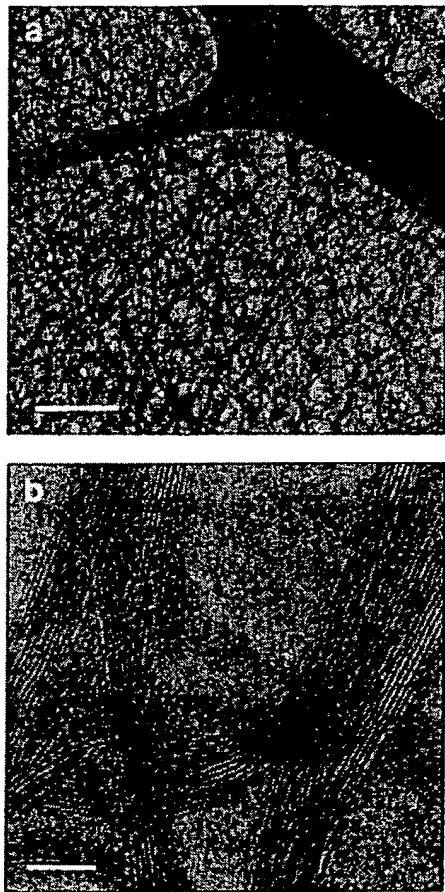

Fig. 2. TEM micrographs at low (a, scale bar 0.2 mm) and high (b, scale bar 20 nm) magnification of as-synthesized single-shell nanotubes purified by treatment in boiling nitric acid. Microscope Hitachi H9000-NAR, 100 kV. Note: The treated samples are more sensitive to the TEM beam than the original material, probably due to the presence of the oxides.

Large areas of the mat formed by the pure single-shell nanotubes on the TEM grids revealed no severe damage to the walls of the nanotubes, as shown in Figure 2b. The nitric acid not only reacts preferably with the particles but it leaves most of the tubes intact in the bundles. Occasionally one can see isolated tubes but it is very difficult to tell whether the tubes are open or not because of the low contrast of a single carbon wall. Some debris can still be seen on the outside of the bundles. Probably, after removing the impurities, the acid reacts with the outermost tubes of the bundles. In other words, the outer tubes in the bundle protect the inner ones.

In this regard, it should also be noted that no distortion or loss of contrast is visible in the TEM pictures of the walls

of the single-shell nanotubes in the purified samples. This could mean that the sp^2 structure is mostly conserved and that the amount of sp^3 carbons bearing alcohol, carboxylic or carbonyl functions is quite small. This is unlike multi-shell nanotubes, where these functional groups are found to cover the entire surface.[6] Nevertheless, those hydrophilic groups are undoubtedly present on the purified single-shell nanotubes since the purified nanotubes are much more stable in aqueous suspensions than the raw ones. Like multishell tubes, annealing of the samples at high temperature should eliminate residual surface oxides.[12]

Although we did not see any remaining catalytic particles in the sample, a chemical analysis was performed on the samples to quantify the amount of metal before and after purification. Interestingly, while the target contained 2 % metal (Ni and Co, total weight percent), the amount in the raw nanotube samples was 3 %. In terms of nanotube content this about 6 %, while purification leaves ca. 1 %. In other words, the metal content is reduced by a factor of six relative to the nanotube content. The 1% is still surprisingly large considering that these metals readily dissolve in the acid. We are currently trying to find ways of removing the remaining metal.

A final remark is warranted. Due to their high curvature, nanotubes pick up impurities from just standing in air or in a solvent. This can be a very fast process, occurring in a day or even less, depending on the environment. It results in the nanotubes being coated with a sheath of amorphous material, which is easily observed by TEM. Needless to say this can have significant consequences on any property measurements.

It seems clear from this study that the kinetics of the reactivity of single-shell nanotubes is different from that of both multishell nanotubes and fullerenes. In particular they are relatively inert toward oxidation by acids, at least in a bundle form. This property allows the purification of the as-synthesized mixture by this fast, high-yield, and easy to handle procedure. This is by far the simplest and most reproducible method to date for both single and multishell tubes. It should be a helpful step for further physical or chemical experiments and technological applications.

Experimental

pH of the successive washing solutions is monitored and is about six when the suspension of single-shell nanotubes starts to be stable on the centrifugation timescale. At this point, the powder is washed twice with 15 mL portions of nitric acid and filtered on fritted glass before rinsing twice with 15 mL portions of distilled water. Between each of these steps the suspension is sonicated. Finally, the wet powder is dried and kept in a dessicator under vacuum. The overall yield ranges between 30 and 50 %.

Synthesis of Single-Shell Nanotubes: A carbon target is made by mixing 31 g of graphite cement (Dylon Industries Inc.) with 2.70 g of graphite powder (GP-G, Dylon Industries Inc.), 0.35 g of cobalt (Aldrich, powder, <2 μm, 99.8 %), and 0.36 g of nickel (Aldrich, powder, submicrometer, 99.8 %).The homogeneous mixture containing 0.3 at.-% of each catalyst is molded in a 0.75 inch quartz tube (1 inch ≈ 2.54 cm) and baked in air for 12 h at 120 °C and for 12 h at 200 °C. The baked target is then cured at 1200 °C for 6 h in vacuum (6×10^{-2} torr). For the nanotube synthesis, the target is placed in a 1 inch quartz tube under a pressure of 500 torr of argon and a gas flow of 400 cm^3/min after several purges. The quartz tube is maintained at 1200 °C during the synthesis. A YAG-Nd laser (SEO Titan-P, 10 Hz, 230 mJ/pulse at 532 nm, 270 mJ/pulse at 1064 nm) was used to generate pulsed beams at 1064 and 532 nm. The former is delayed by 13 ns with respect to the latter. Both beams are focused to a 3–4 mm spot on the target. For optimal yield, the focal spot of the beams is moved on the target every few minutes. After the synthesis runs, the quartz tube is cooled down to room temperature under argon flow. A fine web-like deposit then collects on the walls of the quartz tube and on the cold finger that closes this tube.

[1] T. Guo, P. Nikolaev, A. Thess, D. T. Colbert, R. E. Smalley, *Chem. Phys. Lett.* **1995**, *243*, 49. A. Thess, R. Lee, P. Nikolaev, H. Dai, P. Petit, J. Robert, C. Xu, Y. H. Lee, S. G. Kim, A. G. Rinzler, D. T. Colbert, G. E. Scuseria, D. Tomanek, J. E. Fisher, R. E. Smalley, *Nature* **1996**, *273*, 483.

[2] C. Journet, W. K. Maser, P. Bernier, A. Loiseau, M. Lamy de la Chapelle, S. Lefrant, P. Deniard, R. Lee, J. E. Fischer, *Nature* **1997**, *388*, 756.

[3] S. J. Tsan, M. H. Devoret, H. Dai, A. Thess, R. E. Smalley, L. J. Geerligs, C. Dekker, *Nature* **1997**, *386*, 474.

[4] P. M. Ajayan, T. W. Ebbesen, *Rep. Prog. Phys.* **1997**, *60*, 1025.

[5] T. W. Ebbesen, P. M. Ajayan, H. Hiura, K. Tanigaki, *Nature* **1994**, *367*, 519.

[6] H. Hiura, T. W. Ebbesen, K. Tanigaki, *Adv. Mater.* **1995**, *7*, 275.

[7] S. C. Tsang, Y. K. Chen, P. J. F. Harris, M. L. H. Green, *Nature* **1994**, *372*, 159.

[8] J.-M. Bonard, T. Stora, J.-P. Salvetat, F. Maier, T. Stöckli, C. Duschl, L. Forró, W. A. de Heer, A. Cha<Ü>telain, *Adv. Mater.* **1997**, *9*, 827.

[9] K. Tohji, T. Goto, H. Takahashi, Y. Shinoda, N. Shimizu, B. Jeyadevan, I. Matsuoka, Y. Saito, A. Kasuya, T. Ohsuna, K. Hiraga, Y. Nishina, *J. Phys. Chem.* **1996**, *101*, 1974.

[10] S. Bandow, A. M. Rao, K. A. Williams, A. Thess, R. E. Smalley, P. C. Eklund, *J. Phys. Chem. B.* **1997**, *102*, 8839.

[11] K. L. Lu, R. M. Lago, Y. K. Chen, M. L. H. Green, P. J. F. Harris, S. C. Tsang, *Carbon* **1996**, *34*, 814.

[12] M. Kosaka, T. W. Ebbesen, H. Hiura, K. Tanigaki, *Chem. Phys. Lett.* **1995**, *233*, 47.